Available online at www.sciencedirect.com
SCIENCE DIRECT
Catalysis Today 116 (2006) 354–360
CATALYSIS TODAY
www.elsevier.com/locate/cattod

Nanosized catalysts for the production of hydrogen by methanol steam reforming

T. Valdés-Solís *, G. Marbán, A.B. Fuertes

Instituto Nacional del Carbón (CSIC), c/Francisco Pintado Fe, 26, 33011 Oviedo, Spain

Available online 30 June 2006

Abstract

Nanoparticulate ternary oxides (perovskites and spinels) and mixtures of oxides have been prepared via a template technique using a sodium silicate-based silica xerogel as template. The oxides prepared by this method were tested as catalysts for the methanol steam reforming reaction at 250 °C and a very high space velocity (WHSV = 52–57 h^{-1}). Copper-based catalysts ($CuMn_2O_4$ and $CuCr_2O_4$ spinels or CuO/CeO_2 and CuO/ZnO) exhibit a high activity and selectivity for the steam reforming process, whereas the other formulations employed ($LaFeO_3$, $LaMnO_3$, $NiMn_2O_4$) are not active in the experimental conditions of this work. The favourable effect of increasing the surface area on the activity of the catalysts is clearly observed for $CuMn_2O_4$, which exhibits the highest initial reaction rate and a selectivity to CO_2 formation of over 90%. The catalytic activity values of the copper-based catalysts are similar to or greater than those found in the literature for common methanol steam reforming catalysts including noble metal-based catalysts. Deactivation of the catalysts seems to be independent of the preparation method and can be attributed to the concomitant effect of coke deposition and sintering.

Keywords: Spinel; Template; Methanol steam reforming; Coke deposition; $CuMn_2O_4$

1. Introduction

Hydrogen production systems by the steam reforming of methanol (SRM) constitute a promising technology for energy feeding in portable electronic devices, for decentralized refuelling units for hydrogen-based automobiles or as on-board generation systems for hydrogen-based internal combustion engines or PEM fuel cells [1]. Methanol is an appropriate source of hydrogen because of its high energy density, safe handling and easy synthesis from renewable and fossil fuels [2]. Methanol transformation into gaseous mixtures enriched with hydrogen can be achieved by several reactions such as SRM (R1) [3–6], methanol decomposition (R2) [2,7] and partial oxidation (R3) [8,9]. In many cases, a combination of these reactions ensures the autothermal conditions as in the oxidative steam reforming process (R4) [10,11]:

$$CH_3OH + H_2O \leftrightarrows CO_2 + 3H_2 \quad (R1)$$

$$CH_3OH \leftrightarrows CO + 2H_2 \quad (R2)$$

$$CH_3OH + 1/2O_2 \leftrightarrows CO_2 + 2H_2 \quad (R3)$$

$$CH_3OH + 0.75H_2O + 0.125O_2 \leftrightarrows CO_2 + 2.75H_2 \quad (R4)$$

In the absence of oxygen, a high selectivity towards reaction (R1) is pursued, either by ensuring that reaction (R2) does not occur or by converting the CO produced in this reaction into CO_2 via the water gas shift reaction, described by (R5) [12]:

$$CO + H_2O \leftrightarrows CO_2 + H_2 \quad (R5)$$

Water gas shift catalysts have been proposed for methanol steam reforming because they facilitate the methanol reforming reaction as well as the water gas shift reaction (R5) [12–14]. Perovskites and spinels have been successfully tested as catalysts for the water gas shift reaction [15,16] so that in principle they seem good candidates to be tested for methanol steam reforming. In addition, palladium-based catalysts [4,17,18] or copper-based catalysts promoted by ZnO [6,19], CeO_2 [6,20,21], SnO_2 [22], ZrO_2 [23], Cr_2O_3 [24], ZnO/ZrO_2 [25] or CeO_2/ZrO_2 [26] have proved to be very active in the SRM reaction. Manganese oxides have also been employed as promoters by Idem and Bakhshi [27,28] who discovered that the

* Corresponding author. Tel.: +34 985119090; fax: +34 985297662.
E-mail address: tvaldes@incar.csic.es (T. Valdés-Solís).

0920-5861/$ – see front matter © 2006 Elsevier B.V. All rights reserved.
doi:10.1016/j.cattod.2006.05.063

presence of $CuMnO_2$ and Mn_2O_3 produced an increase in the catalytic activity of the catalyst.

For all the above mentioned structures it is vital to devise preparation techniques that lead to the fabrication of catalysts with a high surface area, whose value is parallel to that of the catalytic activity. However, the common preparation methods of mixed oxides and mixtures of oxides usually require the unconfined precursors to be subjected to high temperature calcination steps. This provokes the sintering of the resulting particles, with the concomitant reduction of active surface area, typically in the range of a few square meters (<10) per gram. Thermal treatments can be avoided by the use of ''chimie douce''-based nanotechnological approaches, such as microemulsion techniques [29], but these are expensive procedures which, moreover, must integrate stages for the separation of the organic solvents and surfactants. These disadvantages, when using thermal methods for unconfined precursors or liquid phase preparations, have been recently overcome by means of nanocasting procedures, such as template methods with hard templates (porous solids such as silica gel and active carbon) [30–32]. In this case, the synthesis of the nanoparticles takes place in a confined space formed by the porosity of the template. The attraction of these methods is the confined calcination process that avoids the uncontrolled growth of the material during the synthesis, thus favouring the formation of nanostructures. Several materials have been prepared by template methods using active carbon [32] and mesostructured silica materials [33]. Recently, our lab used an inexpensive mesoporous silica xerogel template to prepare high surface area single metal oxides [31] as well as high surface area perovskites and spinels [34]. The ternary oxides prepared by this method attain BET surface area values up to 110 m^2/g and particle sizes below 16 nm. The main advantage of using silica xerogels instead of active carbon resides in its stability at high temperatures, since the reactivity of carbonaceous materials in the presence of transition metal oxides can be a drawback (i.e. undesired reduction of oxides). On the other hand, some oxides such as ZnO cannot be prepared with a silica template since they are soluble in the conditions employed to remove the template after calcination. In these cases active carbon must be used instead.

The goal of this work is to prepare high surface area ternary oxides and mixtures of oxides, with special emphasis on copper-based materials, following a nanocasting procedure in which silica xerogel is employed as template. The catalytic activity of the fabricated materials in the production of hydrogen by methanol steam reforming is tested, and the results are then compared to those obtained with catalysts of a similar composition prepared by standard methods reported in the literature.

2. Experimental

2.1. Catalyst preparation. Template technique

The synthesis of nanosized perovskites and spinels by the silica template method has been recently reported [34]. The method has been extended in this work to the preparation of mixtures of oxides (CuO/CeO_2). The procedure for preparing xerogel and oxides is schematically presented here. The silica source (sodium silicate, Aldrich) was added under stirring to an aqueous solution of HCl. The molar composition of the synthesis mixture was sodium silicate/HCl/H_2O = 1/6/194. The solution was stirred in a closed Teflon vessel for 20 h at ambient temperature and subsequently heated to 100 °C for 2 days. The gel was then filtered and washed several times with water and acetone and finally dried at room temperature. To synthesize the metal oxides, a solution of the hydrated metal nitrates in the appropriate ratio was prepared in ethanol (0.4–0.6 M). The silica xerogel was stirred with this solution at moderate temperature (60 °C) until complete removal of the solvent. The impregnated sample was dried at 80 °C overnight and calcined in air at 5 °C/min up to the temperature required for the formation of the oxide and then left for 4 h. The mixed oxides were obtained after the dissolution of the silica framework in a NaOH solution (2 M) and final washing with distilled water to remove impurities. The catalysts prepared in this work are

Table 1
Preparation conditions and characterization of nanoparticulate material (ST: silica template; CT: carbon template; O/T: inputted oxide/template weight ratio)

Reference[a]	Formulation	Method	T_{calc} (°C)	Soaking time (h)	Detected phases (XRD)	D (nm) (XRD)	S_{BET} (m^2/g)
P-LaMn	$LaMnO_3$	ST (O/T = 1.0)	850	4	$LaMnO_3$	13.5	32
P-LaFe	$LaFeO_3$	ST (O/T = 1.0)	700	4	$LaFeO_3$	10.9	110
S-CuCr	$CuCr_2O_4$	ST (O/T = 1.0)	800	4	$CuCr_2O_4$	14.0	90
S-CuMn-a	$CuMn_2O_4$	ST (O/T = 1.0)	550	4	$CuMn_2O_4$	15.6	100
S-CuMn-b	$CuMn_2O_4$	ST (O/T = 0.5)	550	4	$CuMn_2O_4$	7.6	144
S-NiMn	$NiMn_2O_4$	ST (O/T = 1.0)	800	4	$NiMn_2O_4$	14.1	87
MO-CuCe	CuO/CeO_2 (15%/85%)	ST (O/T = 1.0)	650	4	CeO_2	5.6	153
MO-CuZn	CuO/ZnO (50%/50%)	CT (O/T = 0.3)	350	4	CuO, ZnO	9.2 (ZnO)[b]	40
L-CuZnZr	$CuO/ZnO/ZrO_2$ (40%/30%/30%)[c] [25]	Coprecipitation	550	4	CuO, ZnO, ZrO_2[d]	12.6	64
L-CuCeAl	$CuO/CeO_2/Al_2O_3$ (50%/20%/30%) [35]	Coprecipitation	500	3	CuO[d]	11.0	114

[a] P: perovskite; S: spinel; MO: mixture of oxides; L: literature.
[b] 9.1 nm for CuO phase.
[c] Molar ratio.
[d] These phases are coincident with those detected in the original works.

summarized in Table 1, which also contains the experimental conditions of the preparation.

Two different samples of $CuMn_2O_4$ were prepared by modifying the nitrates-to-silica ratio in order to obtain materials of a different particle size and surface area values. CuO/ZnO (50 mol%/50 mol%) was prepared by nanocasting using a mesoporous active carbon as template due to the solubility of ZnO in NaOH.

Additionally, for the sake of comparison, two copper-based catalysts [L-CuZnZr = CuO (40 mol%)/ZnO (30 mol%)/ZrO_2 (30 mol%) and L-CuCeAl = CuO (40 wt.%)/CeO_2 (20 wt.%)/Al_2O_3 (40 wt.%)] prepared by standard coprecipitation and reported to be highly active in SRM [25,35] were also prepared by following the procedures reported by the authors [25,35] and analyzed for the SRM reaction at the conditions used in this work.

2.2. Catalyst characterization

X-ray diffraction (XRD) patterns for the oxide particles were obtained on a Siemens D5000 instrument. The particle size was determined by means of Scherrer's equation. Nitrogen adsorption isotherms were performed at 77 K on a Micromeritics ASAP 2010 volumetric adsorption system. The BET surface area was deduced from the isotherm analysis in the relative pressure range of 0.04–0.20. Transmission electron microscopy (TEM) was performed in a Jeol Mod. 2000 EX II microscope (200 kV). The Raman spectra were recorded with a Horiva (LabRam HR UV) spectrometer.

2.3. Catalytic activity

Catalytic activity experiments were performed with 20 mg of catalyst diluted in 200 mg of SiC particles (<75 μm) in an electrically heated Vycor reactor (7.1 mm i.d.). The catalyst was pre-treated in helium at 250 °C for 60 min (F = 200 cm^3/min). Afterwards the reaction was performed at 250 °C in a mixture of 7.0 vol.% CH_3OH, 7.7 vol.% H_2O in He to balance [F = 200 cm^3/min, WHSV (methanol weight hourly space velocity) = 52–57 h^{-1}]. Methanol and water were injected into the reactor via a syringe pump through a vaporizer. The products (CH_3OH, H_2O, H_2, CO and CO_2) were analyzed on-line by mass spectrometry (Omnistar 300O).

In order to compare the catalytic activity of different catalysts a kinetic approach was adopted using a potential type equation for the reaction rate:

$$r_{SRM} = k' P^{\alpha}_{CH_3OH} P^{\beta}_{H_2O} P^{\gamma}_{H_2} P^{\delta}_{CO_2} \quad (1)$$

As the experiments were carried out under experimental conditions in which water was in excess of methanol and total conversion was relatively low (below 0.2), the effect of water steam, carbon dioxide and hydrogen on the reaction rate can be dismissed and so Eq. (1) can be rewritten as:

$$r_{SRM} = k P^{\alpha}_{CH_3OH} \quad (2)$$

Assuming plug flow in the integral reactor, the continuity equation can be written as

$$r_{SRM}(X, P_{CH_3OH}, P_{H_2O}, P_{H_2}, T) = \frac{F^0_{CH_3OH} dX}{dw_m} \quad (3)$$

In this equation, $F^0_{CH_3OH}$ is the inlet methanol flow (mol/s), dw_m the mass of the catalyst (g) in a differential element of the system, dX represents the methanol conversion in the same element, and r_{SRM} is the reaction rate, expressed in moles of methanol per gram per second, which, after a standard mathematical transformation, can be expressed as:

$$r_{SRM} = \frac{F^0_{CH_3OH}}{w_m} \frac{(1-X)^{\alpha} - (1-X)}{1-\alpha} \quad (4)$$

Finally, the selectivity towards CO_2 formation during the reaction can be evaluated by the following equation:

$$S = \frac{P_{CO_2}}{P_{CO_2} + P_{CO}} \quad (5)$$

3. Results and discussion

3.1. Catalyst preparation and characterization

The nanoparticulate materials prepared in this work are summarized in Table 1. Spinels and perovskites are formed by chemically pure phases as determined by XRD [34]. Structurally, the fabricated materials are made up of porous agglomerates of particles of a size below 16 nm, as detected by TEM inspection. These values are similar to those reported in Table 1, and obtained by the application of Scherrer's equation to the XRD spectra, and also to the values derived from geometrical relationships and S_{BET}, thus confirming the nanoparticle structure [34]. Fig. 1 illustrates the XRD patterns of MO-CuZn and MO-CuCe. The CuO and ZnO phases are present in the MO-CuZn catalyst, whereas the MO-CuCe catalyst only exhibits the CeO_2 phase, which is due to the lower copper content (Cu/Ce molar ratio = 0.18) as a result of which the particle size of the copper phase is smaller.

Additionally, the reference catalysts L-CuZnZr and L-CuCeAl (Table 1) exhibit the XRD crystallographic phases reported in the literature (CuO, ZnO and ZrO_2 for L-CuZnZr [25] and CuO for L-CuCeAl [35]) and particles of relatively small sizes, although they are larger than those obtained by the nanocasting procedure. The particle size and S_{BET} values are presented in Table 1.

In the case of $CuMn_2O_4$ catalysts, two materials (S-CuMn-a and S-CuMn-b) were prepared by changing the amount of the precursor in the impregnating solution (Table 1). It can be observed that the higher the values of the O/T (oxides-to-template) ratio, the larger the particles and consequently the lower the values of the specific surface area. This is probably due to a more complete filling of the pores during the impregnation of the template, in the zone of the higher pore sizes as the O/T ratio increases. This parameter can therefore be used to tailor the final particle size of the oxides formed.

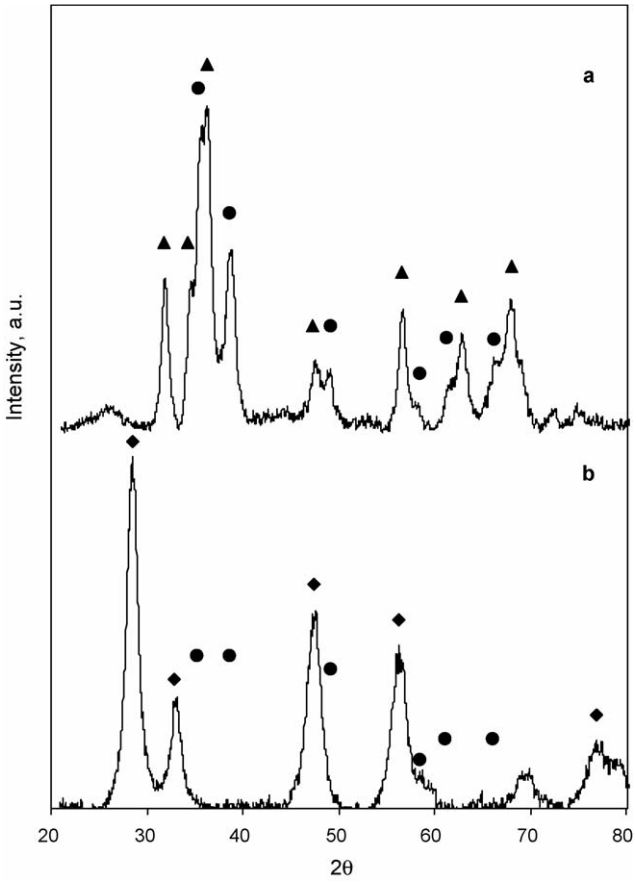

Fig. 1. XRD patterns of the mixtures of oxides prepared by templated technique: (a) MO-CuZn; (b) MO-CuCe; (▲) ZnO zincite; (●) CuO tenorite; (◆) CeO_2 cerianite.

3.2. Catalytic activity and selectivity

The catalytic activity experiments were performed at 250 °C, exerting a slight over-pressure of water steam with respect to the methanol partial pressure. As stated in Section 2 the catalytic activity is expressed in this work by the reaction rate indicated by Eq. (1). Table 2 shows the values of the different coefficients of Eq. (1) extracted from literature. Significant differences are apparent between the values of the coefficients, even for catalysts of a similar composition (i.e. $CuO/ZnO/Al_2O_3$). For copper-based catalysts, the methanol partial pressure exponent (α) shows two main values: 0.6–0.7, when oxidized catalysts are involved, and around 0.27 when reduced catalysts are employed. The water steam partial pressure exponent (β) takes values below 0.4 while that of hydrogen partial pressure (α) takes values between −0.2 and −1. As pointed out in Section 2, the effect of H_2 partial pressure can be neglected in the experimental conditions of this work (low conversion values). To check whether the effect of water steam on the reaction rate can be neglected or not, the numerical resolution of Eqs. (1) and (3) ($\gamma = \delta = 0$) was performed with values of β between 0 and 0.4 for all the experimental and literature conversion values considered in this work. The results of this resolution show that the average relative standard deviation with respect to the $\beta = 0$ reaction rate is quite low (STD = 4.6 ± 7.3%) supporting the validity of the $\beta = 0$ assumption. This assumption favours the reaction rates obtained with high conversion values (literature rates, STD = 7.5 ± 8.6%) with respect to the rates for the catalysts developed in this work, obtained at low conversion values (STD = 0.6 ± 0.6%). Therefore, the reaction rate for SRM was evaluated by means of Eq. (4) with the appropriate selection of the α value (0.65 or 0.27).

In Fig. 2, the values of the reaction rate calculated by Eq. (4) and $\alpha = 0.65$ are plotted versus time on stream for the different catalysts. P-LaMn and P-LaFe (Table 1) are not included because of their negligible reaction rates even at temperatures as high as 350 °C.

Although the initial reaction rate is very high for the S-CuMn-a, S-CuMn-b and MO-catalysts (see Table 3 for comparison), a significant deactivation is clearly appreciated during the SRM experiments. The effect of the specific surface area on the reaction rate can be exemplified by S-CuMn-a and S-CuMn-b. As expected, the catalyst with the higher surface area and the smaller particle size (S-CuMn-b), exhibits a higher reaction rate during the whole experiment than the other catalyst, although the deactivation trends are similar.

The selectivity values for the SRM reaction as evaluated by Eq. (5) are plotted in Fig. 3 for the different catalysts. A more or less marked decrease during time on stream is observed for all

Table 2
Reaction order for the methanol steam reforming reaction

Catalyst	Reference	α	β	γ	δ	H_2O/CH_3OH
$CuO/ZnO/Al_2O_3$	[40]	0.60	0.40	–	–	1.0
$CuO/ZnO/Al_2O_3$	[41]	0.70	0.10	–0.20	–	1.2
Pd/ZnO	[17]	0.72	0.09	–	–	1.8
$CuO/ZnO/Al_2O_3$	[42]	0.63	0.39	−0.23	−0.07	1.2–5.2
$Cu/MnO/Al_2O_3$	[28]	0.28	–		−0.99	1.0
$Cu/ZnO/Al_2O_3$	[43] 170–260 °C	0.26	0.03	−0.20	–	1.0

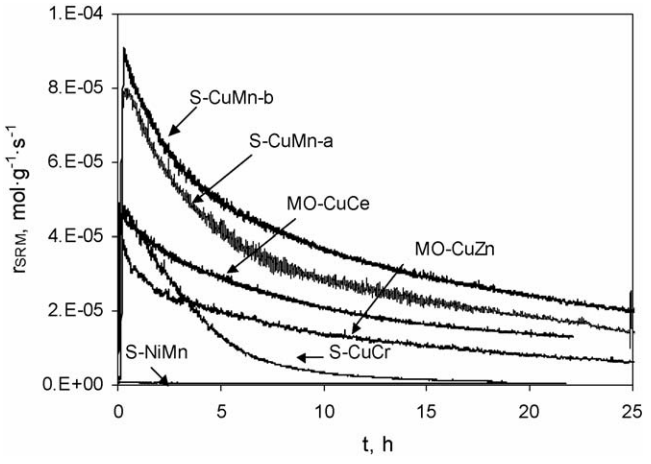

Fig. 2. Reaction rates in the methanol steam reforming process at 250 °C for several nanoparticulate materials (T = 250 °C, α = 0.65, WHSV = 52–57 h^{-1}).

Table 3
Comparison between the reaction rate values (r_{SRM} = mol/(s g)) of the methanol steam reforming reaction for selected catalysts

Catalyst [Reference] (denomination in original work)	T (°C)	TOS (h)	WHSV (h^{-1})	$P^0_{CH_3OH}$ (Pa)	r_{SRM} ($\times 10^5$ mol/(s g))	
					$\alpha = 0.27$	$\alpha = 0.65$
Literature catalysts (noble metals)						
Pd/ZnO [17]	250	n.i.	13.6	25800	6.83	5.30
Pd/ZnO [4] (16.7 wt.% Pd)	254	n.i.	7.7	36477	2.04	1.89
PtZn alloy [5]	280	n.i.	0.5	6282	0.26	0.19
Pd/ZnO [18]	250	30	31.4	6282	14.2	11.80
Literature catalysts (non-noble metals)						
$Cu/ZnO/Al_2O_3$ [44] (CZA)	263	n.i.	20.5	5758	8.04	6.99
$CuO/ZnO/ZrO_2$ [25] (CZZ-433 (550))	250	45	24.4	15705	3.50	3.38
CuO/ZrO_2 [23]	250	n.i.	7.9	50663	1.53	1.45
$CuO/ZnO/Al_2O_3$ [42] (BASF K3-110)	225	n.i.	5.4	43058	1.24	1.16
Cu/ZnO [45] (HP-$Cu/ZnO/Al_2O_3$)	250	25	3.9	19486	2.02	1.16
$Cu/ZrO_2/Al_2O_3$ [46] (15 wt.% ZrO_2)	250	>50	3.3	42298	1.35	1.16
$Cu/Y_2O_3/CeO_2/Cr/Al_2O_3$ [47] (Cu15-Y2Ce10 + 2% CrAl)	250	8	11.7	38971	5.92	3.31
Cu/CeO_2 [6] (3.8 wt.% Cu/CeO_2)	240	24	2.6	40530	0.93	0.83
$CuO/CeO_2/ZrO_2$ [26] ($CuO/CeO_2/ZrO_2$ = 8/1/1)	225	5[a]	3.5	16702	1.89	1.31
CuO/CeO_2 [20] (Cu/Ce = 0.15/0.85; urea/nitrates = 3.3)	240	n.i.	0.9	5066	0.24	0.23
$Cu/MnO/Al_2O_3$ [28] (p-5CM2)	250	n.i.	17	50663	5.53	1.66
Catalysts prepared in this work						
MO-CuCe	250	1	54.4	7120	4.28	4.20
MO-CuCe	250	20	54.4	7120	1.40	1.39
MO-CuZn	250	1	56.6	7120	3.04	3.00
MO-CuZn	250	20	56.6	7120	0.79	0.79
MO-CuZn	250	30	56.6	7120	0.63	0.63
S-CuMn-a	250	1	56.6	7120	7.53	7.28
S-CuMn-a	250	20	56.6	7120	1.86	1.85
S-CuMn-a	250	40	56.6	7120	0.60	0.60
S-CuMn-b	250	1	51.6	7120	8.12	7.81
S-CuMn-b	250	20	51.6	7120	2.41	2.38
S-CuMn-b	250	25	51.6	7120	2.02	2.00

T: reaction temperature; TOS: time on stream; WHSV: methanol weight hourly space velocity; n.i.: not indicated.
[a] No deactivation was observed.

catalysts, signifying that catalyst deactivation exerts a more negative effect on the SRM reaction (R1) than on the methanol decomposition reaction (R2). Taking into account the total duration of the experiments, the best selectivity values are obtained for the copper–ceria catalysts (over 0.97) and for the hopcalite catalysts (over 0.9), whereas MO-CuZn exhibits selectivity values over 0.8 for the whole experiment (25 h) (Fig. 3). The lowest selectivity values are obtained for the catalyst with one of the worst catalytic performances (S-CuCr).

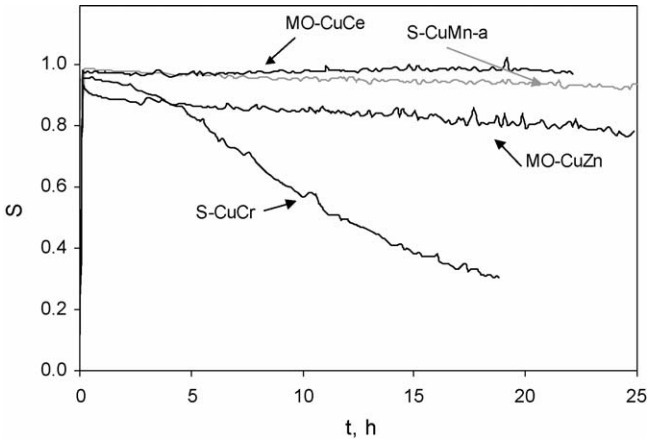

Fig. 3. Selectivity to CO_2 of the nanosized catalysts in the SRM reaction (T = 250 °C, α = 0.65, WHSV = 52–57 h^{-1}).

In Table 3 the values of the reaction rate calculated by Eq. (4) on the basis of literature data reported for a number of catalysts are listed together with those of the catalysts prepared in this work. Two values of α corresponding to the two ranges observed in the literature were used in the calculations. The table includes both noble metal-based catalysts and non-noble metal-based catalysts. The reaction rate values presented in Table 3 in most cases are hardly affected by the value of the α coefficient, so that both sets of values lead to the same conclusions. As can be seen, palladium-based catalysts present the highest reaction rate values, even at the most stringent conditions (WHSV = 31.4 h^{-1}). The set of non-noble metal-based catalysts presents a wide range of reaction rate values, from 0.24×10^{-5} to 8.04×10^{-5} mol/(s g) ($\alpha = 0.65$), the highest values being comparable to those of Pd-based catalysts. However, there is no clear correlation between activity and composition for the non-noble metal (copper)-based catalysts. The values of the initial reaction rate (1 h) for the nanoparticulate catalysts prepared in this work are comparable to the highest values reported for the literature catalysts, with a maximum value of 8.12×10^{-5} mol/(s g) for S-CuMn-b.

3.3. Catalyst deactivation

Deactivation during the methanol steam reforming process is commonly attributed to a change in oxidation state, catalyst sintering, coke deposition or poisoning of the catalyst by foreign species in the feed (i.e. chloride, sulphur, etc.) [36]. Since purified laboratory mixtures are used in the feed and deactivation rate caused by a change in the oxidation state should be faster than the rate shown in Fig. 3, sintering and coke deposition appear to be the most probable causes of deactivation in this case. However, copper catalysts are sometimes considered to be resistant to coke deposition [36] and sintering seems improbable at the low temperature used for reaction.

To determine whether catalyst deactivation was caused in this work by of the specific reaction conditions under which the experiments were performed (helium diluted methanol and water streams at 250 °C), a selection of catalysts previously reported as stable in the literature were prepared and tested at the same experimental conditions as those used in this work. Matter et al. [25], by using a $CuO/ZnO/ZrO_2$ catalyst (L-CuZnZr), showed that steady state was reached after 10 h in stream (250 °C, 15 vol.% CH_3OH, 19.4 vol.% H_2O, WHSV = 24.4 h^{-1}), whereas for the $Cu/CeO_2/Al_2O_3$ catalyst (L-CuCeAl) designed by Zhang and Shi [35] the steady state was attained at around 40 h (250 °C, 41.7 vol.% CH_3OH, 41.7 vol.% H_2O, WHSV = 3.3 h^{-1}). Catalysts with the formulations proposed by these groups were prepared in our lab following the coprecipitation procedures described in their works [25,35]. As suggested by Matter et al. [25], no catalyst pre-reduction was carried out before the activity measurements were performed under the conditions established in this work, in order to achieve the stationary state in a shorter time. The results of these activity experiments are plotted in Fig. 4, together with those obtained for S-CuMn-a and MO-CuCe. It can be seen that the catalysts considered previously as stable undergo an even greater degree of deactivation than the catalysts prepared in our work. It can be deduced, therefore, that deactivation was probably not detected in the original works [25,35] because it was concealed by the experimental conditions under which the catalysts were initially tested. This would seem to rule out sintering as a cause of deactivation, since the reaction temperature was similar in all cases, although specific gas compositions might obviously catalyze or decelerate sintering. On the other hand, the reaction rate for coke deposition, which is probably a consequence of CO disproportionation [37], must be affected by the partial pressures of the reactants and also by the space velocity, which is very high for the conditions used in this work.

The possible formation of coke deposits was checked by means of Raman spectroscopy. Fig. 5 displays the Raman spectra of catalysts L-CuZnZr and S-CuMn-a obtained before and after the steam reforming process. For L-CuZnZr broad bands centred at about 1370 and 1540 cm^{-1} appeared after 16 h of reaction time, confirming the presence of coke deposits on the surface of the catalyst [38,39], whereas only a broad band centred at about 1520 cm^{-1} was evident for S-CuMn-a. Air oxidation of the deactivated catalysts at 250 °C for long times (over 40 h) produced a partial recovery of the initial catalytic activity, although not to the original level. In this case, the remaining deactivation must be attributed to either active phase sintering or stabilized coke deposits that survived the air oxidation treatment.

To promote the stability of the catalysts, new approaches are currently under study, intrinsically linked with the predominant cause of deactivation. Oxidative methanol steam reforming (R4) could constitute the best solution, as the presence of oxygen in the reforming gases would reduce or even suppress coke formation, and at the same time improve the energy balance at the expense of an acceptable loss of hydrogen. Modifications to the experimental conditions are also being considered as thermodynamic calculations show that a decrease in coke formation can be attained by increasing the H_2O/CH_3OH ratio (readily attainable) and by increasing the reaction temperature, although this would favour the sintering of the active phase and would be detrimental to an eventual implementation of the process.

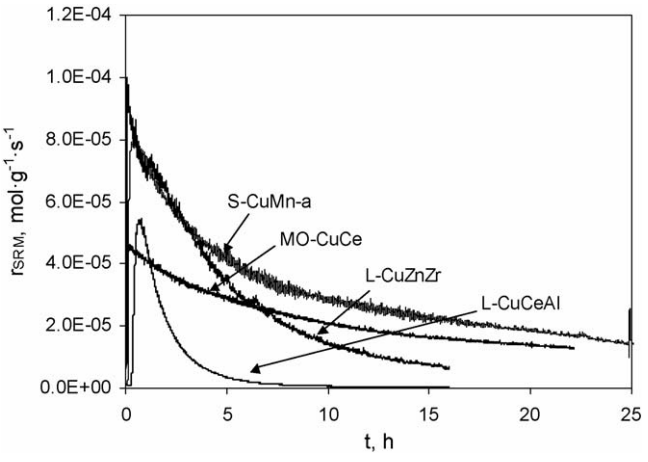

Fig. 4. Comparison of reaction rates for catalysts of proven stability and nanoparticulate catalysts, tested under the experimental conditions used in this work (T = 250 °C, α = 0.65, WHSV = 52–57 h^{-1}).

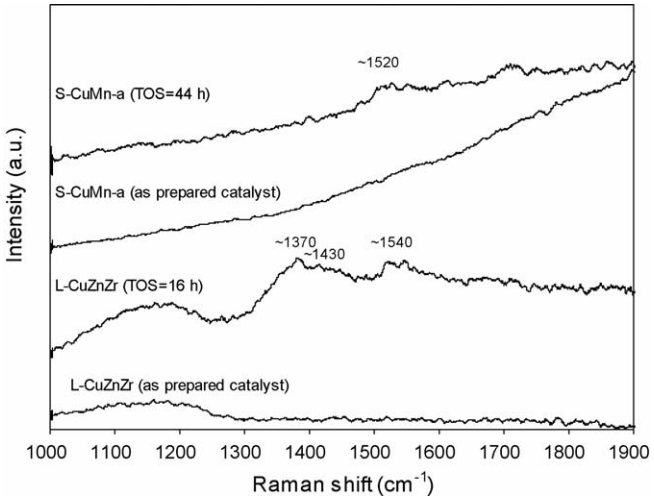

Fig. 5. Raman spectra of the L-CuZnZr and S-CuMn-a catalyst before and after the steam reforming process (T = 250 °C, WHSV = 52–57 h^{-1}).

4. Conclusions

In this work nanoparticulate catalysts prepared by nanocasting techniques were tested for hydrogen production by the steam reforming of methanol. The catalysts which are made up of nanoparticles of a size below 16 nm present pure active phases. The improved surface area provided by this method makes it possible to attain higher initial catalytic activities in the SRM process at 250 °C (WHSV = 52–57 h^{-1}) than by using other catalysts reported in literature. Perovskite catalysts are inactive in SRM, while $CuMn_2O_4$ and CuO/CeO_2 have proven to be the best formulations for this process, showing a catalytic activity, in terms of reaction rate, similar to that of the best catalysts found in literature, with selectivities towards CO_2 formation above 90%. The deactivation undergone by the catalysts seems to be related to the specific feed composition and space velocity used in this work, and may be attributed to coke formation and to a certain degree of active phase sintering. Deactivation would also appear to be independent of the method used to prepare the catalyst.

Acknowledgments

TVS thanks the CSIC-ESF for the award of an I3P postdoctoral contract. Funding by Spanish National Project MAT2005-00262 is also acknowledged.

References

[1] P.J. de Wild, M.J.F.M. Verhaak, Catal. Today 60 (2000) 3.
[2] Y. Matsumura, K. Tanaka, N. Tode, T. Yazawa, M. Haruta, J. Molec. Catal. A: Chem. 152 (2000) 157.
[3] J. Agrell, H. Birgersson, M. Boutonnet, J. Power Sources 106 (2002) 249.
[4] Y.H. Chin, Y. Wang, R.A. Dagle, X.S. Li, Fuel Proc. Technol. 83 (2003) 193.
[5] S. Ito, Y. Suwa, S. Kondo, S. Kameoka, K. Tomishige, K. Kunimori, Cat. Comm. 4 (2003) 499.
[6] Y. Liu, T. Hayakawa, T. Tsunoda, K. Suzuki, S. Hamakawa, K. Murata, R. Shiozaki, T. Ishii, M. Kumagai, Top. Catal. 22 (2003) 205.
[7] J.C. Brown, E. Gulari, Cat. Comm. 5 (2004) 431.
[8] J. Agrell, K. Hasselbo, K. Jansson, S.G. Jaras, M. Boutonnet, Appl. Catal. A: Gen. 211 (2001) 239.
[9] F.W. Chang, H.Y. Yu, L. Selva Roselin, H.C. Yang, Appl. Catal. A: Gen. 290 (2005) 138.
[10] S.T. Liu, K. Takahashi, K. Uematsu, M. Ayabe, Appl. Catal. A: Gen. 277 (2004) 265.
[11] S. Velu, K. Suzuki, M. Okazaki, M.P. Kapoor, T. Osaki, F. Ohashi, J. Catal. 194 (2000) 374.
[12] B.A. Peppley, J.C. Amphlett, L.M. Kearns, R.F. Mann, Appl. Catal. A: Gen. 179 (1999) 31.
[13] D.G. Löffler, S.D. McDermott, C.N. Renn, J. Power Sources 114 (2003) 15.
[14] B.A. Peppley, J.C. Amphlett, L.M. Kearns, R.F. Mann, Appl. Catal. A: Gen. 179 (1999) 21.
[15] Y. Tanaka, T. Utaka, R. Kikuchi, K. Sasaki, K. Eguchi, Appl. Catal. A: Gen. 242 (2003) 287.
[16] K. Sekizawa, S. Yano, K. Eguchi, H. Arai, Appl. Catal. A: Gen. 169 (1998) 291.
[17] C.S. Cao, G. Xia, J. Holladay, E. Jones, Y. Wang, Appl. Catal. A: Gen. 262 (2004) 19.
[18] Y. Suwa, S. Ito, S. Kameoka, K. Tomishige, K. Kunimori, Appl. Catal. A: Gen. 267 (2004) 9.
[19] Y. Choi, H.G. Stenger, Appl. Catal. B: Environ. 38 (2002) 259.
[20] J. Papavasiliou, G. Avgouropoulos, T. Ioannides, Cat. Comm. 5 (2004) 231.
[21] Y. Liu, T. Hayakawa, K. Suzuki, S. Hamakawa, T. Tsunoda, T. Ishii, M. Kumagai, Appl. Catal. A: Gen. 223 (2002) 137.
[22] E.K. Lee, H.S. Kim, K.D. Jung, O.S. Joo, Y.G. Shul, React. Kinet. Catal. Lett. 81 (2004) 177.
[23] H. Purnama, F. Girgsdies, T. Ressler, J.H. Schattka, R.A. Caruso, R. Schomäcker, R. Schlogl, Catal. Lett. 94 (2004) 61.
[24] L. Ma, B. Gong, T. Tran, M.S. Wainwright, Catal. Today 63 (2000) 499.
[25] P.H. Matter, D.J. Braden, U.S. Ozkan, J. Catal. 223 (2004) 340.
[26] H. Oguchi, T. Nishiguchi, T. Matsumoto, H. Kanai, K. Utani, Y. Matsumura, S. Imamura, Appl. Catal. A: Gen. 281 (2005) 69.
[27] R.O. Idem, N.N. Bakhshi, Ind. Eng. Chem. Res. 34 (1995) 1548.
[28] R.O. Idem, N.N. Bakhshi, Chem. Eng. Sci. 51 (1996) 3697.
[29] A. Weidenkaff, Adv. Eng. Mater. 6 (2004) 709.
[30] F. Schüth, Angew. Chem. Int. Ed. 42 (2003) 3604.
[31] A.B. Fuertes, J. Phys. Chem. Sol. 66 (2005) 741.
[32] M. Schwickardi, T. Johann, W. Schmidt, F. Schüth, Chem. Mater. 14 (2002) 3913.
[33] B. Tian, X. Liu, H. Yang, S. Xie, C. Yu, B. Tu, D. Zhao, Adv. Mater. 15 (2003) 1370.
[34] T. Valdés-Solís, G. Marbán, A.B. Fuertes, Chem. Mater. 17 (2005) 1919.
[35] X.R. Zhang, P. Shi, J. Mol. Catal. A: Chem. 194 (2003) 99.
[36] M.V. Twigg, M.S. Spencer, Top. Catal. 22 (2003) 191.
[37] S. Lee, Methanol Synthesis Technology, CRC Press, Florida, 1990, p. 27.
[38] A.B. Fuertes, T.A. Centeno, J. Mater. Chem. 15 (2005) 1079.
[39] F. Tuinstra, J.L. Koenig, J. Chem. Phys. 53 (1970) 1126.
[40] H. Purnama, T. Ressler, R.E. Jentoft, H. Soerijanto, R. Schlögl, R. Schomäcker, Appl. Catal. A: Gen. 259 (2004) 83.
[41] P. Reuse, A. Renken, K. Haas-Santo, O. Gorke, K. Schubert, Chem. Eng. J. 101 (2004) 133.
[42] S.R. Samms, R.F. Savinell, J. Power Sources 112 (2002) 13.
[43] C.J. Jiang, D.L. Trimm, M.S. Wainwright, N.W. Cant, Appl. Catal. A: Gen. 93 (1993) 245.
[44] J. Agrell, H. Birgersson, M. Boutonnet, I. Melián-Cabrera, R.M. Navarro, J.L.G. Fierro, J. Catal. 219 (2003) 389.
[45] T. Shishido, Y. Yamamoto, H. Morioka, K. Takaki, K. Takehira, Appl. Catal. A: Gen. 263 (2004) 249.
[46] X.R. Zhang, P. Shi, J. Zhao, M. Zhao, C. Liu, Fuel Proc. Technol. 83 (2003) 183.
[47] W.H. Cheng, I. Chen, J.S. Liou, S.S. Lin, Top. Catal. 22 (2003) 225.